Molecular Biology of the Cell
Vol. 20, 3261–3272, July 15, 2009

Plasma Membrane Area Increases with Spread Area by Exocytosis of a GPI-anchored Protein Compartment

Nils C. Gauthier,*† Olivier M. Rossier,*† Anurag Mathur,‡ James C. Hone,‡ and Michael P. Sheetz*

Departments of *Biological Sciences and ‡Mechanical Engineering, Columbia University, New York, NY 10027

Submitted January 23, 2009; Revised April 10, 2009; Accepted May 8, 2009
Monitoring Editor: Howard Riezman

The role of plasma membrane (PM) area as a critical factor during cell motility is poorly understood, mainly due to an inability to precisely follow PM area dynamics. To address this fundamental question, we developed static and dynamic assays to follow exocytosis, endocytosis, and PM area changes during fibroblast spreading. Because the PM area cannot increase by stretch, spreading proceeds by the flattening of membrane folds and/or by the addition of new membrane. Using laser tweezers, we found that PM tension progressively decreases during spreading, suggesting the addition of new membrane. Next, we found that exocytosis increases the PM area by 40–60% during spreading. Reducing PM area reduced spread area, and, in a reciprocal manner, reducing spreadable area reduced PM area, indicating the interconnection between these two parameters. We observed that Golgi, lysosomes, and glycosylphosphatidylinositol-anchored protein vesicles are exocytosed during spreading, but endoplasmic reticulum and transferrin receptor-containing vesicles are not. Microtubule depolymerization blocks lysosome and Golgi exocytosis but not the exocytosis of glycosylphosphatidylinositol-anchored protein vesicles or PM area increase. Therefore, we suggest that fibroblasts are able to regulate about half of their original PM area by the addition of membrane via a glycosylphosphatidylinositol-anchored protein compartment.

INTRODUCTION

A fundamental question about cell behavior is whether cells control their plasma membrane area upon spreading, migration, or division; and, if so, how modulation in plasma membrane area can affect these processes. Most animal cells continually change their shape rapidly during migration or division. The plasma membrane (PM) area could physically limit shape changes because the membrane is inelastic and area changes are thought to be slow (Morris and Homann, 2001; Sheetz *et al*., 2006). This raises the question of whether the PM increases in area when cells spread from sphere to disk on matrix-coated substrates (Dubin-Thaler *et al*., 2004). Previous studies have suggested that there might be a large increase (300%) in fibroblast PM area upon spreading (Kehle and Herzog, 1989). Measurements, however, were indirect and based on fixed samples. Two very recent studies addressed similar questions with different results. An increase in PM area was reported for spreading *Dictyostelium* cells; however, a 10-fold lower increase (only 20–30%) was recorded (Traynor and Kay, 2007). In contrast, no detectable changes in PM area were reported between fully spread and early suspension monkey epithelial cells (Boucrot and Kirchhausen, 2007). However, in the same study, an extremely large increase in PM area during mitosis between metaphase and cytokinesis (240–600% depending on cell types) was observed (Boucrot and Kirchhausen, 2007).

Intracellular compartment dynamics and mechanisms involved in the modulation of membrane surface area are poorly understood. Some proteins have been shown to move to the cell surface upon shape changes caused by migration, spreading, or mitosis, and in some cases, indirectly correlated with a possible regulation of PM area (Bretscher and Aguado-Velasco, 1998; Rappoport and Simon, 2003; Schmoranzer *et al*., 2003; Proux-Gillardeaux *et al*., 2005). For example, it has been shown that post-Golgi vesicles are exocytosed toward the leading edges of migrating fibroblasts (Bergmann *et al*., 1983; Schmoranzer *et al*., 2003; Schmoranzer and Simon, 2003) and LY exocytosis is required for PM repair after wounding (Reddy *et al*., 2001; Andrews and Chakrabarti, 2005). However no study has clearly established if the PM area is altered during cell spreading and which compartment is involved.

In the present study we use accurate measurements of membrane area and tension to test whether the PM is increased during cell spreading. We also examined which intracellular compartments are responsible for PM regulation during cell spreading.

This article was published online ahead of print in *MBC in Press* (http://www.molbiolcell.org/cgi/doi/10.1091/mbc.E09–01–0071) on May 20, 2009.

† These authors contributed equally to this work.

Address correspondence to: Michael P. Sheetz (ms2001@columbia.edu).

Abbreviations used: BFA, brefeldin A; ER, endoplasmic reticulum; LY, lysosome; PM, plasma membrane; TIR-FM, total internal reflection fluorescence microscopy; tfr, transferrin receptor; WGA, wheat germ agglutinin.

MATERIALS AND METHODS

Cell Culture Transfection and Reagents

HeLa cells, immortalized mouse embryonic fibroblasts RPTPα (Giannone *et al*., 2004), and NIH-3T3 fibroblasts were cultured in DMEM with 10% fetal bovine serum or 10% newborn calf serum for NIH-3T3 cells and 10 mM L-glutamine in an atmosphere of 5% CO_2 and 95% air (all products from Invitrogen, Carlsbad, CA). One day before experiments, cells were plated to minimize cell–cell interactions before replating for spreading assays. FuGENE 6 (Roche Diagnostics, Basel, Switzerland) was used to transfect the eukaryotic plasmids when cell where plated. Constructions used in this work were as follows: yellow fluorescent protein (YFP)-Golgi, red fluorescent protein-endoplasmic reticulum (RFP-ER) (Clontech, Mountain View, CA), GPI-

green fluorescent protein (GFP) and lysosomal-associated membrane protein (Lamp1)-GFP (from A. Galmiche, Institut für Medizinische Strahlenkunde und Zellforschung, University of Würzburg, Würzburg, Germany). Alexa-568–coupled mouse transferrin (Invitrogen) was loaded to the cell at 20 μg/ml as FM1-43 for the "FM1-43 before spreading" assay (see below). The calcium ionophore A23187 was from Sigma-Aldrich (St. Louis, MO).

Membrane Tension Determination by Optical Tweezers

The cells were viewed by a video-enhanced differential interference contrast (DIC) microscope (Carl Zeiss MicroImaging, Thornwood, NY) equipped with laser optical tweezers (Kuo and Sheetz, 1992). Carboxylated, 1-μm-diameter latex beads (Polysciences, Warrington, PA) were coated with concanavalin A by use of carbodiimide linkage (Kuo and Sheetz, 1993). Beads were attached to the cell membrane and pulled away from the cell surface to form a membrane tether. The tether force was calculated from the displacement of the bead from the center of the laser tweezers during tether formation and the calibration of the trap (Dai and Sheetz, 1995). Membrane tension was related to the square of the tether force as deduced from the lipid bilayer systems (Hochmuth *et al*., 1996).

Spreading Assay

Cells were detached with trypsin/EDTA (0.05% for 2 min; Invitrogen), and the trypsin was then inactivated with soy bean trypsin inhibitor (1 mg/ml in DMEM; Invitrogen), (Sigma-Aldrich). The cells were then suspended in Ringer's solution (150 mM NaCl, 5 mM KCl, 1 mM $CaCl_2$, 1 mM $MgCl_2$, 20 mM HEPES, and 2 g/l glucose, pH 7.4) and incubated for at least 30 min before plating on coated surfaces. Coverglasses were acid washed, treated with hexamethyldisilazane (Sigma-Aldrich), and coated or not with 10 μg/ml fibronectin (2 h in phosphate-buffered saline [PBS] at 37°C; Roche Diagnostics, Mannheim, Germany).

PM Area Measurement

N-(3-triethylaminoniumpropyl)-4-(4-(dibutylamino) styryl) pyridinium dibromide (FM1-43) or 1,1′-didodecyl-3,3,3′,3′-tetramethylindocarbocyanine perchlorate (DiIC12) were prepared following the manufacturer's recommendations (Invitrogen). Cells were spread on fibronectin precoated coverslips (10 μg/ml; 2 h in PBS at 37°C for total internal reflection fluorescence microscopy [TIR-FM] recording of DiIC12 uptake and epifluorescence recording of FM1-43 uptake) or fibronectin-coated 35-mm plastic dishes (25 μg/ml; 2 h in PBS at 37°C, for epifluorescence recording of DiIC12 uptake). Cells were washed three times with ice-cooled Ringer's solution and incubated for 25 min on ice in Ringer-DiIC12 (2 μM) or Ringer-FM1-43 (4 μM). For FM1-43 uptake, cells were rapidly transferred to an IX81 inverted microscope (Olympus Imaging America, Center Valley, PA). DIC and epifluorescence images were captured for <5 min at 0°C using a 20 × objective (UPlan Apo 20 × 0.80 numerical aperture [NA] oil). A Roper Scientific CoolSNAP fx cooled charge-coupled device (CCD) camera (Photometrics, Tucson, AZ) recorded 16-bit digital grayscale images from the microscope. For $DiC1_2$ uptake, after three washes with ice-cooled Ringer's solution, cells were analyzed with the same microscope used for the FM1-43 before spreading assay. A mercury burner associated with a 488-nm excitation filter was used to record the epifluorescence intensity. Texas Red-coupled wheat germ agglutinin (WGA) (4 μg/ml in Ringer's solution) was prepared following the manufacturer's recommendations (Sigma-Aldrich), and the dye was used following the same protocol developed for the DiIC12.

FM1-43 before Spreading Assay

FM1-43 was prepared following the manufacturer's recommendations (Invitrogen). Cells were loaded with DMEM-FM1-43 (4 μM) for 30 min at 37°C. Subsequently, a modified protocol of the spreading assay was used. FM1-43 was added (4 μM) to the Ringer's solution for 30 min during the cell suspension step. After three washes, the cells were plated in Ringer's solution onto a fibronectin precoated coverslip (10 μg/ml; 2 h in PBS at 37°C). The cell spreading was recorded with a custom-designed prism-based TIR-FM microscope by using an upright BX-50 microscope (Olympus Imaging America) coupled to the 488-nm excitation light from a argon-ion laser (Melles Griot Lazer Group, Carlsbad, CA). Cells were visualized with a 20 × objective (XLUMPlanFI 20 ×/0.95 W; Olympus Imaging America). A Roper Scientific CoolSNAP fx cooled CCD camera (Photometrics) recorded 16-bit digital grayscale images from the microscope.

FM1-43 during Spreading Assay

A modified protocol of the spreading assay was used. FM1-43 was added (8 μM) to the Ringer's solution for 1 min at the end of the cell suspension step. Fibronectin precoated coverslip (10 μg/ml; 2 h in PBS at 37°C) were incubated with Ringer-FM1-43 (8 μM) for 1 min at 37°C. The cells were plated on the coverslip in Ringer-FM1-43 (8 μM). DIC and epifluorescence images were captured on an IX81 inverted microscope (Olympus Imaging America), with a 40 × objective (UApo/340 40 × 1.35 NA oil iris; Olympus Imaging America). A high-sensitivity Cascade II camera (Photometrics) was used to minimize light-induced toxicity to the cells. To measure endocytosis, cells were washed with Ringer's solution for 30 s at 37°C and then with iced-cooled Ringer's solution for the amount of time indicated in each experiment. For nocodazole (Sigma-Aldrich) treatments (5–10 μM), cells were incubated in Ringer-nocodazole, or in Ringer-dimethyl sulfoxide (DMSO) (Sigma-Aldrich) as a control, during the 30 min in suspension. Cells were plated for spreading in Ringer-nocodazole-FM1-43 or Ringer-DMSO-FM1-43. DMSO was always used at 1 μl/ml, corresponding to the volume of DMSO-nocodazole for 10 μM nocodazole treatments. The same protocol was used for brefeldin A (BFA; Sigma-Aldrich) treatment (18 μM) with methanol as a solvent.

Substrate Preparation and Microcontact Printing

Silicon wafers were spin coated with a polymethyl methacrylate resist and baked for 5 min at 250°C. The resist was e-beam patterned with an FEI XL 30 Sirion scanning electron microscope (Sirion Therapeutics, Tampa, FL) and treated with a vapor-phase fluorosilane to facilitate removal of the polydimethylsiloxane (PDMS) stamp. The master was designed with four rectangular regions of circles with different diameters (3, 5, 10, 20, 30, 40, and 50 μm). Glass coverslips no. 1.5 (Corning Life Sciences, Acton, MA) were cleaned for 1 h in a 3:1 concentrated H_2SO_4:30% H_2O_2 ("piranha") solution, rinsed thoroughly with deionized water, and dried by rinsing in acetone and baking at 130°C for 10 min. Then, 2.5 nm of a 60/40 silver-palladium alloy was deposited on a 1.5-nm Ti adhesion layer via e-beam evaporation using a Semicore SC2000 evaporation system immediately after cleaning. PDMS stamps were prepared using a Sylgard 184 silicone elastomer kit (Dow Corning, Midland, MI) by pouring a 10:1 solution of elastomer to initiator over the master and curing overnight at 60°C. For each substrate, the stamp was dipped in a 2 mM ethanolic solution of HS-C18 thiol, dried with argon gas, and placed in contact with the substrate for 1 min, after which the substrate was soaked for 2 h in 2 mM ethanolic solution of $HS\text{-}C_{11}EG_3$ thiol to render the nonstamped areas nonadhesive. Samples were rinsed with ethanol, dried with argon, and stored at 4°C until the fibronectin coating. One to 5 d before an experiment, substrates were incubated for 1.5 h with 10 μg/ml full-length FN (Roche Diagnostics) at 37°C and rinsed with PBS. Substrates are kept at 4°C until use.

Image Analysis and Statistics

The microscopes were controlled by the Simple PCI software (Compix, Sewickley, PA). All images were analyzed using the free-access ImageJ software (http://rsb.info.nih.gov/ij/). A whole cell fluorescence level was quantified as follows: a wide area containing one cell was selected from the 16-bit epifluorescence recording, and the intensity of an identical area in the same field but without cells was subtracted from that value, to obtain only the fluorescence intensity of the cell. When a sequential acquisition was performed, the same protocol was followed for each time point. The values of fluorescence in the figures are presented with arbitrary units (A.U.). In Figure 2, fluorescence intensity surface plot analysis was done with the 8-bit images sequentially presented in Supplemental Video 1. For all the assays, substrate contact area of the cell was manually measured from the DIC or epifluorescence patterns of cells. The graphs were plotted using Excel software (Microsoft, Redmond, WA). Student's t test used for all the statistics is the "two samples assuming unequal variances" also from Excel software (Microsoft). The α level was 0.05. The two-tailed p value was used.

RESULTS

PM Tension Decreases during Cell Spreading

The process of cell spreading on a substrate-coated surface generally occurs in four phases (Figure 1A) (Dubin-Thaler *et al*., 2004; Giannone *et al*., 2004). Assuming the PM area is constant during the spreading process, a simple model predicts that spreading from sphere to disk would deplete membrane folds and increase membrane tension (Raucher and Sheetz, 2000). To directly test this model, laser tweezers (Kuo and Sheetz, 1992) were used to pull membrane tethers (Dai and Sheetz, 1998) (Figure 1B) on fibroblasts during the different phases of spreading. Contrary to the predictions of a simplistic model, PM tension decreased during spreading from 16.2 to 6.8 pN (Figure 1A). This finding could be explained if cells increased their PM area as they spread.

PM Area Increases during Cell Spreading

A range of substrate contact areas was obtained by incubating sparsely plated cells for 5 and 30 min on the same coverslip. To measure PM area, cells were loaded with the membrane dyes FM1-43 (Brumback *et al*., 2004) or DiIC12 (Honig and Hume, 1989) at 4°C, to stop exocytic and endocytic events during the dye binding process (Figure 1, C and

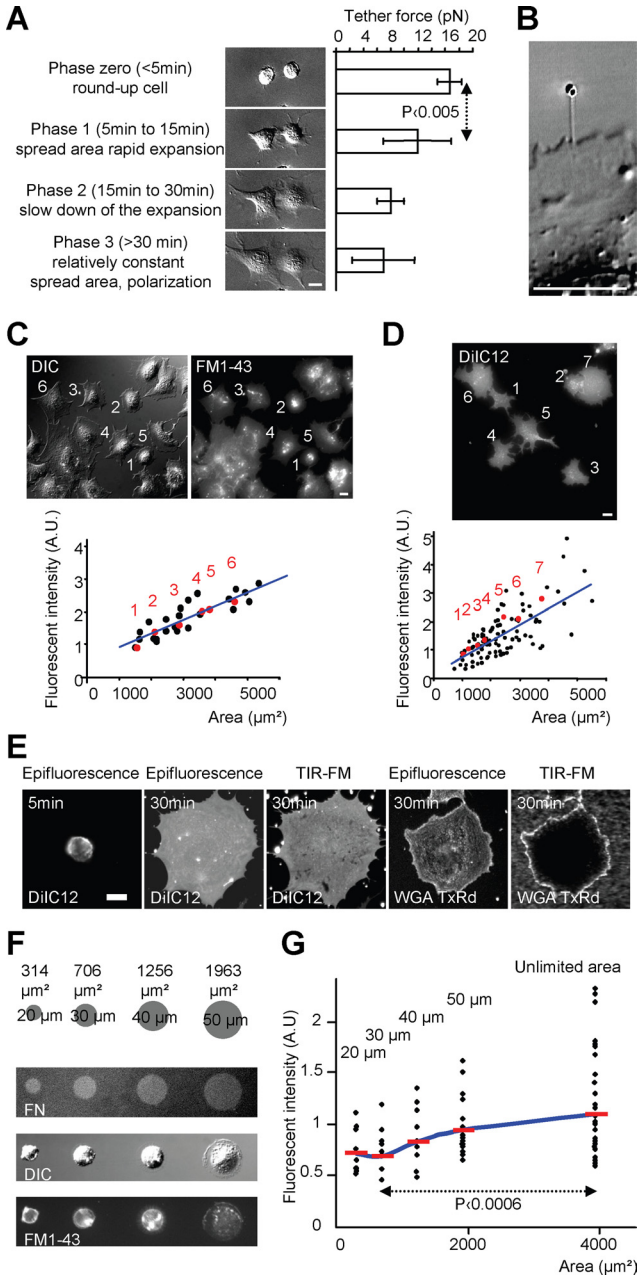

Figure 1. Cell spreading is accompanied by a decrease in PM tension and an increase in PM area, increase proportional to substrate contact area. (A) Average tether forces (at least 5 tethers from different cells) in NIH-3T3 cells during the spreading phases (Dubin-Thaler *et al.*, 2004; Giannone *et al.*, 2004). Error bars, SD (B) DIC image of a tether pulled from an RPTPα fibroblast. Scale, 5 μm. (C) DIC and epifluorescence acquisition of RPTPα cells after incubation at 4°C with FM1-43. Bar, 10 μm. The numbered cells are presented in the graph in which FM1-43 fluorescence intensity (representing PM area) was plotted as a function of substrate contact area for 30 RPTPα cells from one typical experiment. Fitting line is in blue. (D) Same as panel C but only epifluorescence acquisition with DiIC12 dye for 100 RPTPα cells. (E) TIR-FM analysis of the cells was performed, revealing that DiIC12 efficiently labeled the PM area facing the coverslip, during the acquisitions performed at 4°C. WGA was unable to stain that part of the PM. (F) Example of patterned circles coated with fibronectin (FN) onto which cells has been spread for 45 min and incubated at 4°C with FM1-43. (G) FM1-43 fluorescence intensity (representing total PM area) was plotted as a function of substrate contact area for one typical experiment. Each black dot represents a cell. Mean fluorescence intensity, red dashes; best fit for mean fluorescence intensity, blue line. For unlimited substrate contact area, the plotted area represents the average of substrate contact areas on that region.

D). FM1-43 is a useful probe to track membrane area and exocytosis (Smith and Betz, 1996) due to its 350-fold greater fluorescence in membranes than in solution and its inability to cross cell membranes (Brumback *et al.*, 2004). Because FM1-43 staining is reversible (Brumback *et al.*, 2004), the dye was maintained in the media during rapid image acquisition. DiIC12 remains in the membrane for long periods, allowing imaging after free dye is washed away. A linear relationship between substrate contact area and PM area was observed with both staining approaches (Figure 1, C and D). When the substrate contact area doubled, PM area increased by 78 ± 4% (SEM; n = 5, FM1-43 staining), suggesting a close correlation between PM area and substrate contact area. Because cells were different in size, this linear relationship could be explained if the cells assumed a similar geometry upon spreading for all cell sizes.

To determine whether PM area increased during cell spreading, regardless of cell size, an average PM area after 5 min of spreading was compared with that after 30 min (Figure 1E). For mouse embryonic fibroblasts (RPTPα), substrate contact area increased fourfold between 5 and 30 min (from 665 ± 164 to 2588 ± 782 μm^2 [mean ± SD], 100 cells for each time point; n = 3), whereas PM area increased 41.6 ± 1.7% (SEM; n = 3). For NIH-3T3 fibroblasts analyzed after 5 and 60 min of spreading (NIH-3T3 cells spread slower than RPTPα), substrate contact area increased 6.5-fold (from 290 ± 78 to 1905 ± 607 μm^2 [mean ± SD], 100 cells for each time point), whereas PM increased 63.9% (100 cells for each time point). Thus, we found that spreading involved a dramatic increase in PM area.

Substrate Contact Area Affects PM Area

If the substrate contact area was related to PM area, limiting matrix contact area could limit PM area. Microcontact printing (Chen *et al.*, 1997) was used to pattern fibronectin-coated circles of different areas onto a nonadhesive background (Figure 1F and Supplemental Figure 1). We found that PM area increased with the substrate contact area above a threshold of 706 μm^2 (Figure 1G). Moreover, the PM area increased by 53 ± 6% (Figure 1G; SEM; n = 2 independent experiments; 45 min of spreading) for cells that spread on continuously coated fibronectin regions, compared with cells spread on 30-μm-diameter circles (706 μm^2; Figure 1G and Supplemental Figure 1). This value was similar to that observed for spreading from 5 to 30 min (i.e., a 41.6% increase in PM area). Thus, the increase in PM area for fully spread cells is related to final substrate contact area when cells spread over ~1000 μm^2.

Membrane Exocytosis Increases PM Area during Cell Spreading

To determine whether increased exocytosis of membrane could account for the increase in PM area, FM1-43 release from cells preloaded with the dye was visualized using TIR-FM (see Figure 2A for protocol) (Schmoranzer *et al.*, 2000). During spreading, FM1-43-preloaded vesicles were observed fusing with the PM (Figure 2B and Supplemental Video 1). A single peak of fluorescence was observed when a vesicle approached the membrane (Figure 2, C and D). This was immediately followed by an increase in the width of the fluorescence peak and a decrease in its maximum intensity, which signified diffusion of the FM1-43 from the fusion site. Such events demonstrated that exocytosis of single vesicles added new membrane during cell spreading; however, the total amount of membrane exocytosed could not be accurately quantified in term of PM area added.

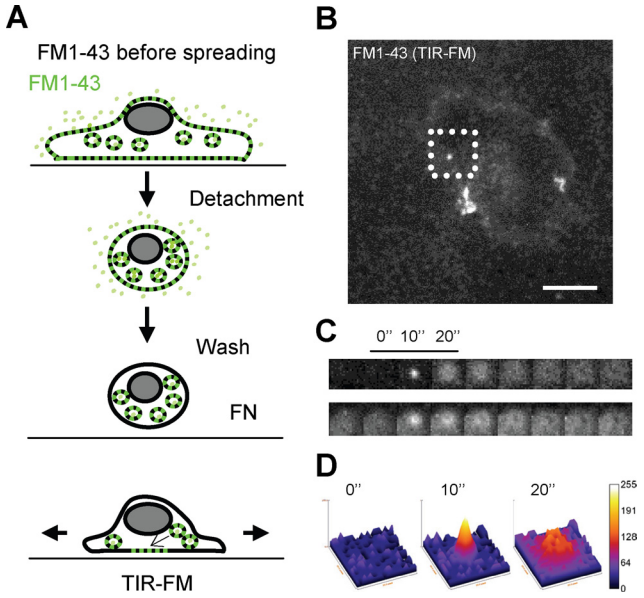

Figure 2. Membrane exocytosis occurs during cell spreading. (A) Schematic representation of the FM1-43 before spreading protocol (see *Materials and Methods*). (B) Example of RPTPα cell TIR-FM images during spreading. Bar, 10 μm. (C) Sequential presentation of two vesicle fusions with the PM extracted from the Supplemental Video 1 (square selection from b is presented in the top row). (D) Fluorescence intensity surface plot analysis of the vesicle fusion presented in the top row of C. Height and colors range represents intensity.

To accurately measure the increase in PM area over time via exocytosis at an individual cell level, cells were incubated with FM1-43 during the spreading and total FM1-43 fluorescence level was monitored for each cell by epifluorescence microscopy (see Figure 3A for protocol used). Immediately after addition of the FM1-43, the fluorescence intensity reported the PM area of the rounded cell before spreading. During spreading, the slope of the FM1-43 fluorescence intensity increased dramatically for ~5–15 min followed by a decreased rate of increase and eventually saturation at 30 min (Figure 3, B and C, Supplemental Figure 2, and Supplemental Video 2). This indicated that there was significant addition of unlabeled membrane through exocytosis. On average, between 5 and 30 min of RPTPα cell spreading (5 and 60 min for NIH-3T3 cells; see Supplemental Figure 2 and Supplemental Video 3), the FM1-43 fluorescence intensity increased by 76 ± 9% (SEM; n = 10) (112 ± 7%, n = 3 for NIH-3T3), indicating that a membrane area equal to at least 76% (112% for NIH-3T3) of the original PM area was exocytosed. That FM1-43 labeling was saturated after labeling of internal membranes (seen as the increased fluorescence in the juxtanuclear region) indicated that there was progressive loading of internal compartments that eventually recycled back to the surface when fully loaded with FM1-43 (Figure 3, B and D, and Supplemental Figure 2). After 30 min, a rapid washing of the cells removed all FM1-43 staining from the PM, enabling quantification of the amount of endocytosis (Figure 3, B and C). By subtracting the endocytosis from the total cell fluorescence just before washout, the PM area of the spread cell was determined. Finally, by comparing PM area before and after spreading, PM area added during spreading was measured. For the three cells presented (Figure 3B), increases in PM area by 17.1% (cell A), 33.5% (cell B), and 52.5% (cell C) were measured, giving a 34.4% increased on average. Again, the estimated PM area increase approximates that observed for spreading from 5 to 30 min (i.e., a 41.6% increase in PM area).

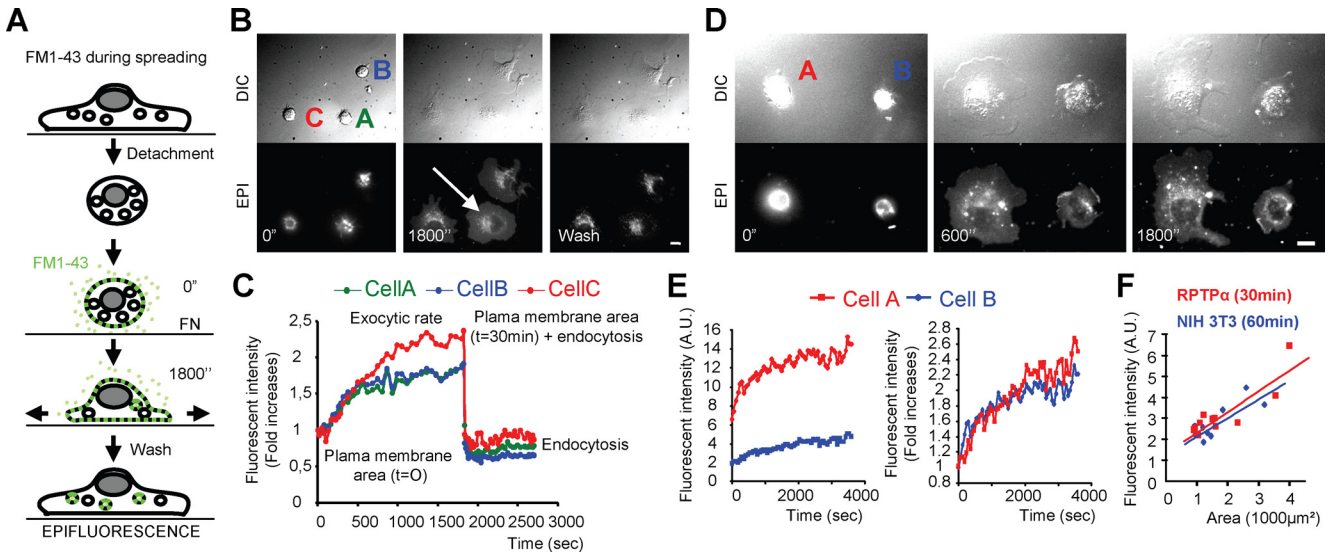

Figure 3. PM area increase is due to the balance between exocytosis and endocytosis. (A) Schematic representation of the FM1-43 during spreading protocol (see *Materials and Methods*). (B) RPTPα cells using the FM1-43 during spreading protocol. Arrow, perinuclear region brightening showing endocytosis. Bar, 10 μm. (C). FM1-43 fluorescence intensity (-fold increases, compared with the initial FM1-43 fluorescence intensity at t = 0″) of each cells plotted as a function of time. (D) Same as B, but without wash and for cells presenting a significant difference in size. (E) FM1-43 fluorescence intensity and fluorescence intensity -fold increases plotted as a function of time for each cell presented in D. (F) Substrate contact area plotted in function of the initial PM area (represented by the FM1-43 fluorescence intensity at t = 0″) after 30 min of spreading for RPTPα cells (red dots and red fitting line; n = 10) and 60 min of spreading for NIH-3T3 cells (blue dots and blue fitting line; n = 10).

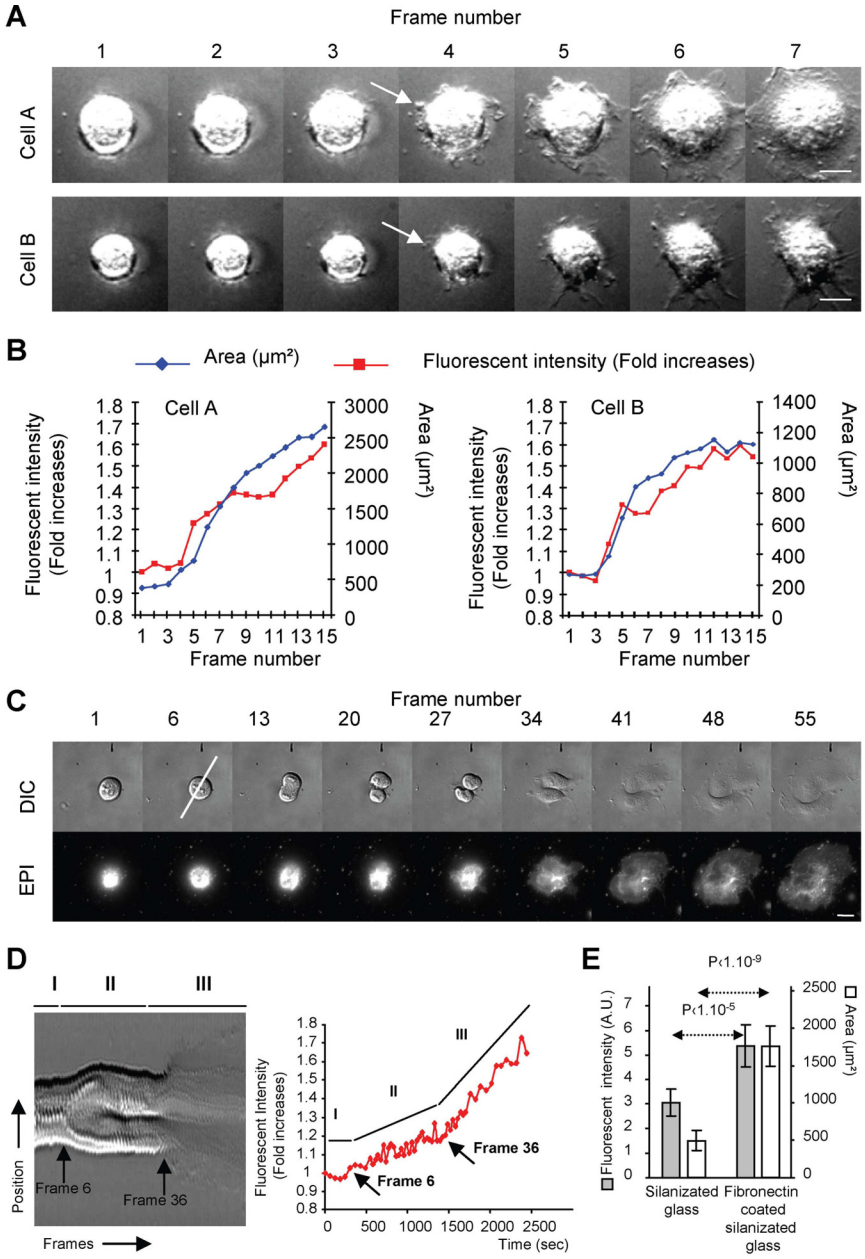

Figure 4. Membrane exocytosis is induced by spreading. (A) Consecutive seven DIC frames acquired at 120-s intervals presented sequentially for two NIH-3T3 cells (Supplemental Figure 2 and Supplemental Video 3). The arrows point to the first expansions presented by the cells. Bar, 10 μm. (B) FM1-43 fluorescence intensity (-fold increase) and substrate contact area of the two cells plotted as a function of frame number. (C) Images of RPTPα cell analyzed with the FM1-43 during spreading protocol during mitosis and postmitotic spreading. Bar, 10 μm. (D) Left, kemograph analysis of the line depicted in C. Different stages of cell division can be identified: before anaphase (I), anaphase to cytokinesis (II), and postmitotic spreading (III). Right, FM1-43 fluorescence intensity -fold increases plotted as a function of time. The three cell division stages correspond to three exocytosis rates: no exocytosis (I), moderate exocytosis (II), and rapid exocytosis (III). (E) NIH-3T3 cells analyzed using the FM1-43 during spreading protocol, after 60 min of spreading from uncoated or fibronectin-coated regions of the same coverslip. Averages of FM1-43 fluorescence intensity and area per cell are presented. Errors bars, SD. n = 50 cells from a typical experiment.

When the PM area of each cell was compared with the amount of area increase and final spread area, we observed that cells with a smaller original membrane area exocytosed less membrane and had a smaller substrate contact area at 30 min (Figure 3, D and E, and Supplemental Figure 2). Furthermore, in both cell lines studied, a linear relationship was observed between PM area before spreading and final substrate contact area (Figure 3F). However when the relative amount of exocytosis was calculated as the percentage increase of the initial PM area, all cells showed a similar percentage increase over time (Figure 3E and Supplemental Figure 2). Thus, we propose that for a wide range of original cell sizes, a similar increase in PM area occurred upon spreading.

Cell Spreading Induces an Exocytic Burst of Membrane

An important question was whether spreading induced membrane exocytosis. Closer examination of NIH-3T3 cell spreading revealed that an exocytic burst occurred as substrate contact area increased (Figure 4, A and B, and Supplemental Video 3). Moreover, FM1-43 uptake by NIH-3T3 cells after 60 min of spreading on fibronectin was 78 ± 17% (SEM; n = 3) greater than cells on the same coverslip that did not spread because the substrate lacked fibronectin (Figure 4E and Supplemental Figure 2).

To further measure this in other cell spreading processes, RPTPα cells were observed during mitosis and postmitotic spreading (Figure 4C and Supplemental Video 4). It was established that exocytosis was greatly reduced during mitosis and that it resumed during the constriction of the mitotic ring at cytokinesis (Strickland and Burgess, 2004); however, no direct quantification of PM area addition has been provided at a single cell level (Strickland and Burgess, 2004). We observed no membrane addition until the cell entered anaphase and started cytokinesis (Figure 4D, stage I). A constant exocytic rate was then observed giving an

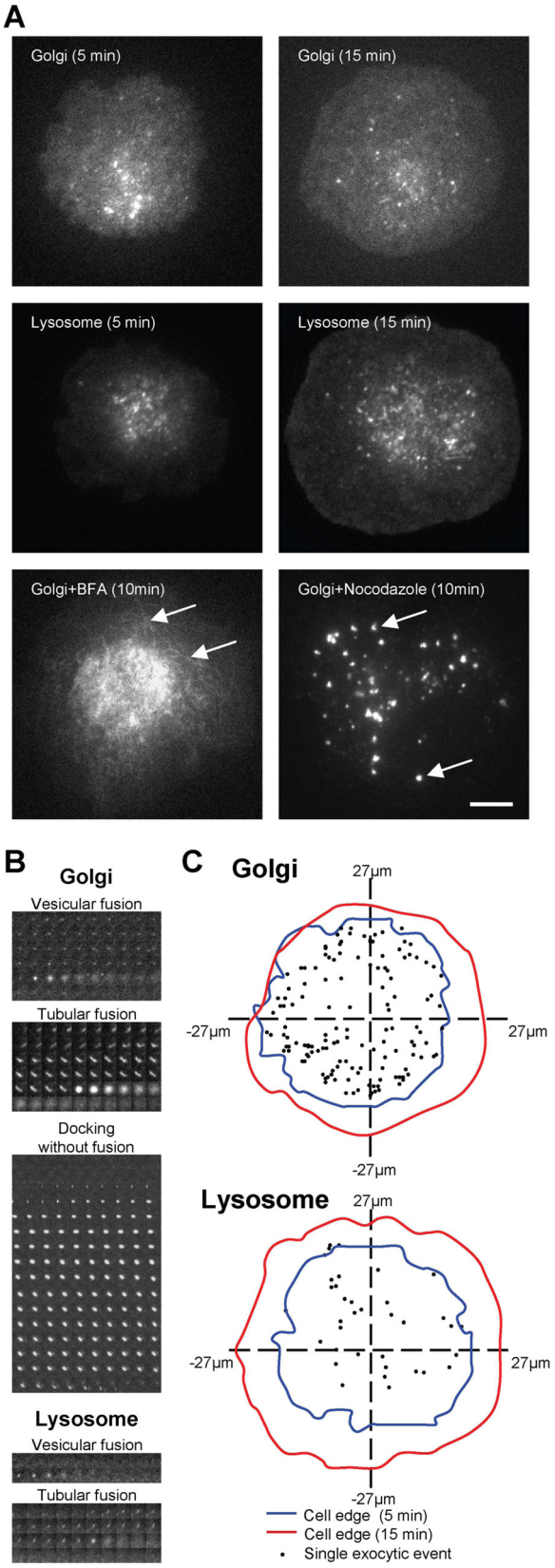

Figure 5. Microtubule-dependent exocytosis of Golgi and LY occurs during spreading. (A) Examples of TIR-FM images for YFP-Golgi– or GFP-Lamp1 (LY)–expressing cells at 5 and 15 min of spreading. Arrows shows the tubular aspect of the Golgi compartment under BFA treatment and its disperse vesicular aspect under nocodazole. Bar, 10 μm. (B) Sequential presentation of different vesicle behaviors analyzed with TIR-FM. Images were recorded every 0.25 s for YFP-Golgi and 0.33 s for GFP-Lamp1. (C) Spatial mapping of all the recordable exocytic events occurring for the cells presented in A.

addition of almost 31 ± 7% (SEM; n = 3) of the initial PM area (Figure 4D, stage II), until the two daughter cells began postmitotic spreading. At that point, a sharp increase in the exocytic rate was recorded (Figure 4D, stage III), further indicating that cell spreading induced an exocytic burst of membrane. These three observations support the idea that the spreading process stimulated additional PM exocytosis.

Golgi and LY Exocytosis Do Not Participate Directly in PM Area Increases during Cell Spreading

We then tried to determine which membrane compartments contributed the most to the increase in area. It has been shown that post-Golgi vesicles are exocytosed toward the leading edges in migrating fibroblasts (Schmoranzer *et al*., 2003; Schmoranzer and Simon, 2003) and that LY exocytosis is required for PM repair after wounding (Reddy *et al*., 2001; Andrews and Chakrabarti, 2005). Those two vesicle populations seemed to be good candidates to provide the increase in PM area during spreading. A yellow fluorescent protein fused with the N-terminal 81-amino acid portion of the human β1,4-galacosyltransferase (YFP-Golgi, Figure 5A) region, containing the membrane-anchoring signal peptide, and a green fluorescent protein fused with the LY-associated membrane protein 1 (GFP-Lamp1, Figure 5A) were expressed to follow vesicles from the transmedial region of the Golgi apparatus and LY, respectively. TIR-FM was then used to monitor vesicle exocytosis during cell spreading. Docking followed by fusion of vesicular and tubular compartments was observed with both constructs, indicating that Golgi and LY exocytosis occurred during spreading (Figure 5B and Supplemental Videos 5 and 6). An accounting of the recorded exocytic events (Figure 5C) during the first 10 min of spreading showed that there were almost 10 times as many Golgi-derived vesicle exocytosis than lysosomal vesicle exocytosis events (11.92 ± 2.52 fusions/min, SEM, n = 4 cells for YFP-Golgi; 1.39 ± 0.46 fusions/min, SEM, n = 11 cells for GFP-Lamp1). In both cases, all the exocytic events occurred in a region 4–5 μm back from the leading edge (Figure 5C) and this boundary correlated with the limit of microtubule extension during the spreading process (Supplemental Figure 3).

Numerous studies have implicated microtubules both in the transport of secretary cargo from the Golgi to the PM (Lippincott-Schwartz and Zaal, 2000) and in late-endosome/LY motility toward the microtubule-organizing center (Matteoni and Kreis, 1987). However, microtubule transport's role in membrane delivery was unclear and controversial given the lack of direct and accurate membrane measurements (Small *et al*., 2002). We found that depolymerization of microtubules with nocodazole (Peterson and Mitchison, 2002) (Supplemental Figure 3) caused an almost total inhibition of Golgi exocytosis (1.4 ± 1.2 fusion/min, SEM, n = 3 cells) (Figure 5A and Supplemental Video 7) and a total inhibition of Lamp1-labeled vesicle exocytosis (no measurable events, 5 cells; Supplemental Video 8). Moreover, in both cases, the vesicles seemed dispersed throughout the cytoplasm and their motility was greatly affected compared with control cases (Supplemental Videos 5 and 6, compared with Supplemental Videos 7 and 8). Nocodazole

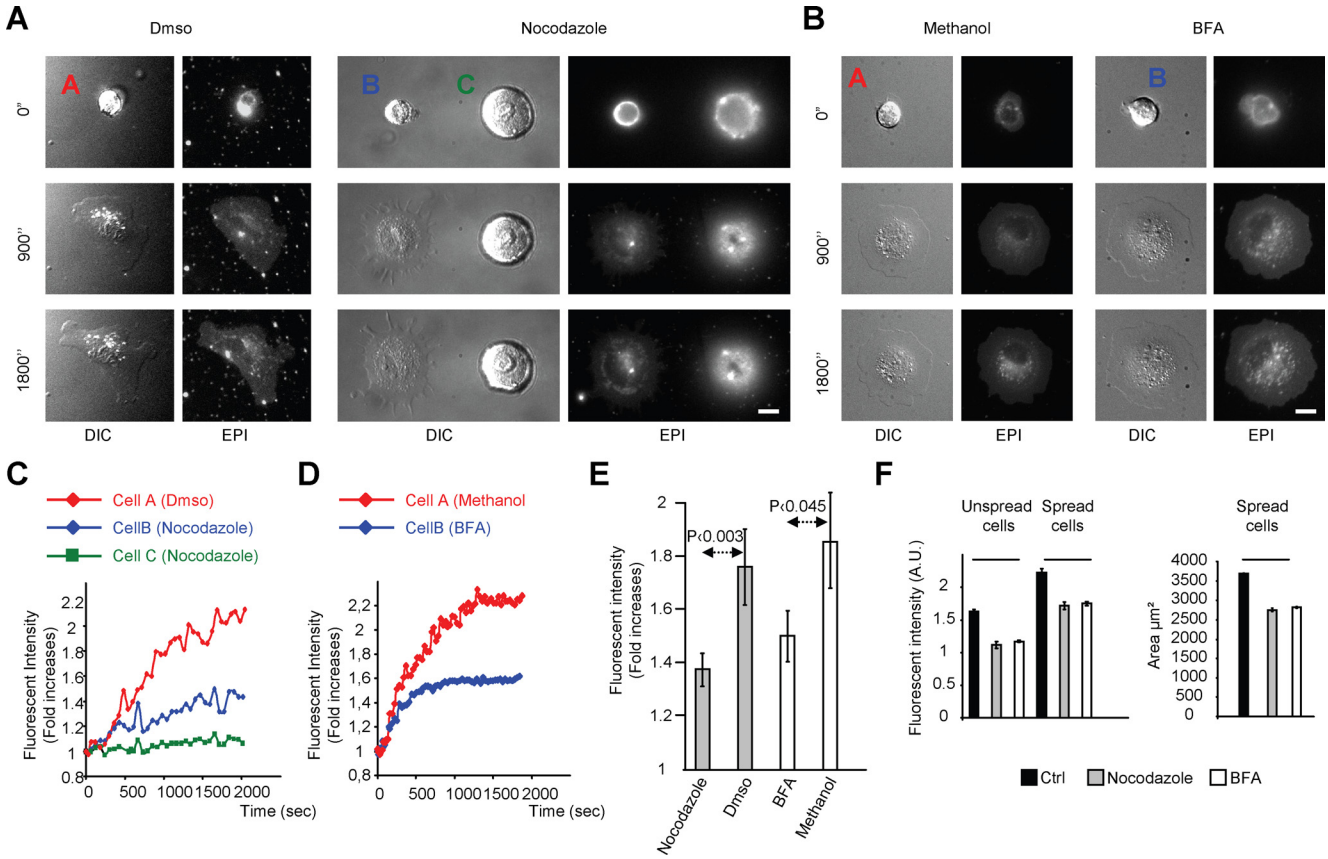

Figure 6. Microtubule-dependent exocytosis participate in plasma membrane homeostasis but not in PM area increase during spreading. (A) Comparison of DMSO (control) and nocodazole-treated RPTPα cells during spreading by using the FM1-43 during spreading protocol. Bar, 10 μm. (B) Comparison of methanol (control) and BFA-treated RPTPα cells during spreading using the FM1-43 during spreading protocol. Bar, 10 μm. (C) FM1-43 fluorescence intensity (-fold increases) of each cell presented in A plotted as a function of time. (D) FM1-43 fluorescence intensity (-fold increases) of each cells presented in B plotted in function of time. (E) Averages of FM1-43 fluorescence intensity (-fold increases) for RPTPα cell after 30 min of spreading. Error bars represent SD between 20 cells from 10 independent experiments (nocodazole or DMSO) or between six cells from two independent experiments (BFA and methanol). (F) Left histogram, FM1-43 fluorescence intensity (representing PM area) of RPTPα cells for unspread cells and 30-min spread cells. Right histogram, area of 30-min spread cells. Each error bar represents the SD of the means for three independent experiments. In each experiment, n = 30 cells (for control [Ctrl], nocodazole, or BFA).

treatment also caused also 47% reduction of spreading-induced exocytosis in RPTPα cells (Figure 6, A, C, and E). The cells spread to a smaller area (Figure 6F) and had more "spiky" edges compared with control cells (Figure 6A and Supplemental Figure 3). Microtubules were also critical for the completion of mitosis (Peterson and Mitchison, 2002). Nocodazole treatment blocked completion of mitosis when applied in metaphase (Figure 6A), and almost no membrane exocytosis was recorded (Figure 6C), reinforcing our previous finding (Figure 4, C and D). In nocodazole-treated NIH-3T3 cells, FM1-43 uptake was also reduced by 49.3% after 60 min of spreading, with a concomitant decrease in the substrate contact area, compared with control cells (Supplemental Figure 3). Because nocodazole treatment affected both Golgi and LY exocytosis, we used BFA to primarily perturb the Golgi exocytosis. In BFA-treated cells, Golgi exocytosis was totally inhibited (no events observed, n = 4 cells; Figure 5A and Supplemental Video 9), but the inhibition seemed different compared with nocodazole treatment. With time, a dispersed Golgi apparatus occurred in the form of a tubular interconnected meshwork characteristic of the heterotypic fusion between ER and Golgi apparatus that occurred after BFA treatment (Lippincott-Schwartz *et al.*, 1989). The exocytic rate of BFA-treated cells was reduced by 45% (Figure 6, B, D, and E), and cells presented a smaller substrate contact area after 30 min of spreading. Given the similar effects of nocadazole and BFA treatment, it seemed reasonable to conclude that the Golgi apparatus was responsible for almost half of the exocytosis that occurred during cell spreading and inhibition of that exocytosis also caused a decrease in the substrate contact area.

Measurements of PM area after 30 min of spreading showed also that both nocodazole and BFA reduced the PM area by a similar amount of 29.6 and 27.2%, respectively (Figure 6F). It was then very tempting to conclude that the Golgi apparatus exocytosis was responsible for the membrane area increase occurring during spreading. Surprisingly, preincubation of the cells in suspension with nocodazole or BFA caused a decrease in the PM area (45 and 38% reduction, respectively; Figure 6F). Moreover, pretreated cells dramatically increased their PM area upon spreading, exhibiting an even greater increase than control cells (54.6% for nocodazole and 49.8% for BFA) (Figure 6F). A closer analysis of the results showed that in both cases the absolute value of the increase in membrane area after spreading was virtually identical to that for control cells (0.596 A.U. for

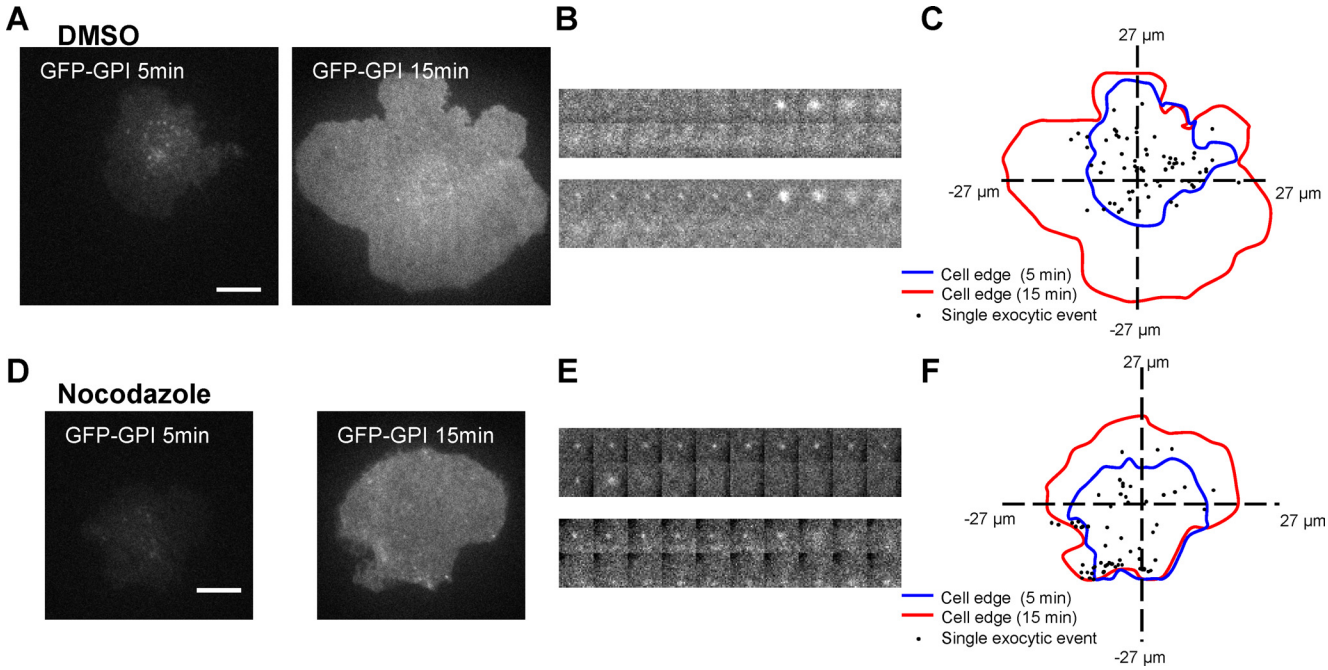

Figure 7. Exocytosis of the GPI-anchored proteins occurs during cell spreading in a microtubule-independent manner. (A) Examples of TIR-FM images for a GFP-GPI–expressing RPTPα cell at 5 and 15 min of spreading in DMSO. Bar, 10 μm. (B) Sequential presentation of two vesicle fusion analyzed with TIR-FM. Images were recorded every 0.14 s. (C) Examples of the spatial mapping of all the recordable exocytic events occurring for the cell presented in A. For D, E, and F, same as above for a nocodazole-treated cell.

control, 0.597 A.U. for nocodazole, and 0.577 A.U. for BFA) (Figure 6F), indicating that similar areas of membrane were added during spreading. Together, these results indicated that blocking Golgi and lysosomal vesicle exocytosis caused a reduction in PM area and in substrate contact area, reinforcing our previous finding that PM area was a critical factor that determined substrate contact area. However, that the same amount of PM was still added during spreading strongly indicated that neither the Golgi apparatus nor the LY were responsible for the PM area increase during spreading. Other compartments were then investigated.

Exocytosis of the Glycosylphosphatidylinositol-anchored Protein Compartment Occurs during Cell Spreading in a Microtubule-independent Manner

At least three other distinct trafficking pathways communicate with the PM. Vesicles from the ER have been described to fuse with the PM at the site of phagocytic cup formation (Gagnon *et al.*, 2002). The two other vesicular populations are part of recycling pathways. One of those recycling pathways involves clathrin-dependent endocytosis. The molecular marker usually used to track this pathway is the transferrin receptor (tfr) (Benmerah and Lamaze, 2007). The other pathway, less understood, is the recycling pathway of molecules entering the cell by clathrin-independent endocytosis (Mayor and Pagano, 2007). Clathrin-independent endocytic routes are highly dependent on cholesterol and the actin cytoskeleton. Common molecules in that pathway are the GPI-anchored proteins (Mayor and Pagano, 2007). Moreover, GPI-anchored protein recycling seems to be different from the recycling pathway followed by the tfr (Naslavsky *et al.*, 2004).

We investigated which of these three trafficking pathways could regulate the PM area increase during spreading. Such a pathway should have the following two characteristics. First, exocytic events should occur with a reasonable frequency to explain the amount of membrane added upon cell spreading. Second, the exocytosis should be microtubule independent as observed for the area increase during spreading.

The ER was fluorescently labeled by expressing a *Discosoma* sp. Red fluorescent protein fused at its N terminus with the ER targeting sequence of calreticulin and at its C terminus with the ER retention sequence KDEL (DsRed-ER). During cell spreading, no exocytic events were recorded (no events observed, n = 3 cells; Supplemental Video 10).

To follow the tfr recycling, cells were preloaded with Alexa-568–coupled transferrin. However, most of the PM was uniformly labeled in TIR-FM. To increase the contrast between labeled internal vesicles and PM, we first photobleached the PM and then recorded exocytic events during spreading (Supplemental Video 11). Only rare exocytic events of transferrin-labeled vesicles were recorded during cell spreading (0.1 event/min; n = 2 cells).

Finally, to follow the GPI-anchored protein exocytic pathway, we expressed a GPI-GFP construct, consisting of the GPI anchoring part of the CD55 decay accelerating factor (DAF) fused with GFP (Gauthier *et al.*, 2005). As for transferrin, the PM was uniformly labeled. Instead of photobleaching to reduce PM fluorescence, we used the fact that the GFP form (F64L/S65T mutant) of our GPI-GFP construct was highly pH sensitive in a reversible manner (Kneen *et al.*, 1998). The reversible pH sensitivity of our construct was confirmed in these cells (Supplemental Figure 4). Moreover, we observed that when the external pH was transiently decreased below pH 4, the quenching of the GFP fluorescence was irreversible (Supplemental Figure 4). Exocytosis of vesicles labeled with GPI-GFP were recorded after a brief acidic pH pulse (pH 4 for 45 s) (Figure 7, A–C, and Supplemental Video 12). The exocytic frequency was half of the

Golgi and six times the LY rate of exocytosis (6.4 fusions/min; n = 2 cells). Moreover, we observed that the exocytosis of this compartment was microtubule independent (6.1 fusions/min; n = 2 cells) (Figure 7, D–F, and Supplemental Video 13).

Knowing that under microtubule depolymerization the constitutive secretory pathway through the Golgi was blocked (Figures 5 and 6), we conclude that GPI-anchored proteins are targeted to the PM during cell spreading through their recycling pathway, and we propose that this pathway participates in the PM area increase observed during cell spreading.

DISCUSSION

In our study, we provide parallel measurements of membrane area (an increase by 50%) and membrane tension (a simultaneous decrease by 50%) showing that the two parameters are regulated during spreading and act together to physically affect motility and shape. Moreover, we extend our observation to another important shape change, mitosis. We observed that exocytosis starts at the onset of anaphase and estimate an increase in plasma membrane area by 26% from metaphase to cytokinesis. We also investigate all possible secretory compartments that could regulate plasma membrane area during spreading and accurately quantified the relative exocytosis rate of those compartments to the plasma membrane. Although some of those compartments (like the Golgi apparatus or the lysosomes) clearly affect plasma membrane area, surprisingly, they do not contribute directly to plasma membrane area increases during spreading. Finally, we identify the GPI-anchored protein recycling compartment as a possible candidate for the plasma membrane area regulation during spreading.

PM Tension, PM Area Regulation, and Membrane Reservoir

The apparent tension in the PM decreases with spreading. We speculate that insertion of new membrane and/or a decrease in membrane–cytoskeleton affinity causes the decrease in the apparent tension. This would in turn promote actin-dependent spreading. In agreement with this hypothesis, we observed an increase in PM area upon spreading. Thus, it seems that cells decrease their membrane tension in correlation with an increase in lamellipodia extension. These results reinforce and extend to physiological conditions of previous correlations between a drop in PM tension and an increase in lamellipodia extension rate after addition of a detergent to artificially decrease PM tension (Raucher and Sheetz, 2000). Without the increase in PM area, the cells cannot spread as far.

We use several approaches to accurately measure PM area and membrane turnover at the single cell level during cell spreading. Other studies have focused on the turnover of specific molecules and not global PM area measurements. For example, the Martin Schwartz group (del Pozo *et al.*, 2004) found that the ganglioside GM1, receptor for cholera toxin, is almost an order of magnitude lower in concentration at the surface of suspended cells compared with adherent cells, whereas some proteins remain unchanged (α5 integrin) or increased dramatically (almost 10-fold in the case of CD44). Changes in specific molecules do not address the fundamental magnitude of the changes in the PM. The PM is ~50% lipid bilayer by mass, and, in this sense, we think that the quantification of PM area change upon spreading is critical for further understanding of membrane dynamics. Moreover, the few studies that have focused on PM area regulation during cell spreading or migration came to very different conclusions. Indeed, the estimated increase in PM area ranges from a 20–30% increase in PM area for *Dictyostelium* cells (Traynor and Kay, 2007), to a 300% increase in PM area for L929 fibroblasts (Kehle and Herzog, 1989). For two different populations of mouse embryonic fibroblasts, we measured, on average, approximately a 50% increase in PM area upon spreading, similar to that observed for *Discostelium* upon spreading (Traynor and Kay, 2007). The two methods of measuring the increase used here gave similar values and both were in a linear range for dye binding to membranes. In experiments in the continued presence of FM1-43, the fact that there was almost a twofold increase in fluorescence upon spreading, whereas there was only a 50% increase in PM area implies that endocytosis recovered half of the PM area that was exocytosed. Our results are in agreement with previous observations of continuous loading of a cationic dye with similar properties to FM1-43 that found about a maximum twofold increase in fluorescence in suspended L929 fibroblasts (Coupin *et al.*, 1999). Moreover, if L929 fibroblasts spreading was accompanied by a 300% increase in PM area as described previously (Kehle and Herzog, 1989), we should have observed at least (if no endocytosis occurs) a fourfold increase of FM1-43 fluorescence upon spreading. But in those previous studies (Kehle and Herzog, 1989), no direct lipid area measurements were made and PM area was estimated, by using immunogold labeling of PM glycoproteins.

When spread area is limited, we observe that the membrane area increases only above the threshold contact area. One explanation for the ability to spread at first without increasing area is that during early spreading, cells take membrane from pre-existing PM folds. Consistent with that hypothesis, we observe regions that are labeled intensely with FM1-43 (representing folded membrane) and decrease in intensity as the cells spread (as shown in Supplemental Video 2). The unfolding of the PM reservoirs could give enough membrane to enable cells to spread until they reach the observed threshold value of area. At that point, having a pool of membrane that is available for exocytosis to increase the PM area could enable the cell to further spread. It is interesting to note that the spread area observed (≈1000 μm^2) is roughly the same area in which the activation of contraction has been observed during spreading of the same cell type (Giannone *et al.*, 2004, 2007; Cai *et al.*, 2006). This indicates that there is a link between spread area and cytoskeleton activation that could also involve activation of exocytosis. A further complexity is that above this threshold of area, the cells increased PM area in proportion to their spread area, supporting the idea that cells are able to dynamically respond and adapt to the different areas of matrix-coated surface as observed in studies of cell growth and viability (Chen *et al.*, 1997) or phagocytosis (Champion and Mitragotri, 2006). A full explanation for this threshold value and the feedback between spread area and PM area needs further investigation. The actual signals have not been identified, but there seems to be a physical component that senses the degree of spreading and perhaps elements of the cell geometry (Neves *et al.*, 2008).

Membrane Exchange during Mitosis: Metaphase to Cytokinesis

Cells are round before mitosis, divide, and spread thereafter. The current findings raise a question about the membrane area changes that occur during this process. In mitosis, we found that exocytosis could increase the PM area by 31% maximally between metaphase and cytokinesis. It is interesting to note that this value is very similar to the theoretical

26% increase in surface area that a simple mathematical model predicts for a sphere that divides into two daughter spheres at constant volume (Supplemental Figure 5). This value is also in agreement with the proposed membrane area change during spermatocyte cytokinesis (Dyer *et al*., 2007), studies in which the authors also proposed that no change in volume was observable. However, 26% is far less than what has been described previously (240–600% increases of PM area during cytokinesis) (Boucrot and Kirchhausen, 2007). This discrepancy may be attributed to cell lines (HeLa or BSC-1 cells instead of mouse fibroblasts) or experimental approaches (confocal section reconstruction instead of epifluorescence of bound dye). To check for a possible difference in cell lines, we measured the amount of membrane exocytosis occurring between metaphase and cytokinesis in HeLa cells (Boucrot and Kirchhausen, 2007). We observed on average, a 24.6% (n = 2 cells) increase in membrane fluorescence in HeLa cells (Supplemental Figure 5), a value similar to the observations in fibroblast and in agreement with the mathematical predictions (Supplemental Figure 5). Thus, we suggest that the actual increase in area is ~26% during the progression from metaphase to cytokinesis.

Identification of the Membrane Pool Regulating PM Area during Spreading

To understand which compartment is responsible for the increase in PM, we analyzed the dynamics of several intracellular compartments during spreading. We were unable to observe ER exocytosis during spreading. Although PM-ER fusion seems to explain the increase in PM area during phagocytosis, fibroblasts are not good phagocytic cells and no other case of ER exocytosis has been reported. In addition, there is still controversy over whether ER–PM fusion occurs (Gagnon *et al*., 2002) or does not occur (Touret *et al*., 2005) during phagocytosis. The absence of tfr exocytosis through its recycling pathway is perhaps more surprising. However, cell spreading may constitute a particular state of the cell in which tfr recycling does not occur. Thus, we suggest that both ER and tfr compartments do not contribute to the area increase upon spreading.

We found that Golgi and LY-derived vesicles are exocytosed to the PM upon spreading. That we find almost 10 times more Golgi-derived vesicle exocytosis events than lysosomal vesicle exocytosis events strongly suggests that Golgi is involved in regulating the PM area upon spreading. Moreover, blocking Golgi exocytosis by microtubule depolymerization, or more specifically with BFA treatment, decreases PM area by an extent similar to the increase upon spreading and results in a corresponding reduction in spread area. However, when nocodazole- or BFA-treated cells spread, there is a normal increase in PM area. We suggest that there is a decrease in constitutive secretion from the Golgi that contributes to membrane homeostasis and PM area but the Golgi-derived vesicles are not the major source for the PM area increase upon spreading.

This brings us to the LY. LY are postulated to be recruited to repair membrane wounds through exocytosis activated by rapid and massive entry of extracellular calcium (Reddy *et al*., 2001; Andrews and Chakrabarti, 2005). However, cell wounding is often induced by mechanical injuries, such as cell scratching, laser scissors, or glass needle perforation (Reddy *et al*., 2001; Andrews and Chakrabarti, 2005), and we did not observe wounding during spreading (if a wound occurs, the cell is immediately loaded with FM1-43; Supplemental Figure 2). In previous studies, microtubule depolymerization gave only a "small reduction" in LY exocytosis but "reproducible in several experiments" (Rodriguez *et al*., 1997; Jaiswal *et al*., 2002). However, we observed that LY exocytosis during cell spreading was microtubule sensitive. To determine whether these observations were discrepant, we measured calcium-induced exocytosis of LY after spreading in nocodazole-treated versus control cells and found the same level in both (Supplemental Videos 14 and 15), indicating that the artificially induced calcium-dependent exocytosis of LY was different in nature than spreading-dependent LY exocytosis. Calcium concentration oscillations have also been observed during the spreading process (Itano *et al*., 2003), but those oscillations seem to originate from intercellular stores (such as ER), and it seems that in neuronal cells, intracellular calcium is not required for surface area regulation (Herring *et al*., 1998). Although LY exocytosis during spreading can contribute to the membrane dynamics and/or protein turnover; it seems to be a secondary process not involved in the spreading-dependent increase in PM area. This is in agreement with the lower frequency of exocytic events observed and the fact that LY exocytosis is inhibited by microtubule depolymerization.

Of the possible compartments that can contribute to the microtubule-independent increase in PM area during spreading, the GPI-anchored recycling compartment seems to be a good candidate. Indeed, GPI vesicles are clearly exocytosed during spreading; and more importantly, blocking the biosynthetic pathway through the Golgi apparatus by microtubule depolymerization does not affect the rate of GPI vesicles exocytosis. Thus, during spreading, GPI vesicles are exocytosed from a microtubule-independent recycling pathway. These results are in agreement with a GPI-anchored protein recycling pathway independently of the tfr recycling pathway (Naslavsky *et al*., 2004). Our results are also in agreement with recent studies in which lipid rafts labeled with cholera toxin move back to the PM upon cell spreading (Balasubramanian *et al*., 2007); but, in contrast to this study, they found a dependence upon microtubules. GPI-anchored proteins are concentrated in microdomains enriched in cholesterol that have been described as lipid rafts (Mayor and Pagano, 2007). This also suggests that the CD55-DAF–derived GPI-anchored protein that we follow in our study has a very long half-life and is mainly recycled. This is in agreement with previous observations showing that CD55-DAF has no measurable degradation after 5 h when the biosynthetic pathway through the Golgi was inhibited with BFA (Li *et al*., 2003). Thus, the GPI-anchored protein compartment has characteristics that enable it to be endocytosed when cells are in suspension and exocytosed upon respreading.

There are several the roles that could be played by this spreading-dependent compartment. Previous studies have shown changes in the plasma membrane protein composition; however, expansion of the plasma membrane by 50% could also cause a dramatic change in the lipid composition. Because the expansion of the spread area is contraction and rigidity dependent (Giannone *et al*., 2004), the addition of membrane could play a role in some of the force- and rigidity-dependent changes that have been reported.

Membrane trafficking linked to cell migration is a subject of emerging interest as discussed in a recent review (Jones *et al*., 2006). In addition, over the past 6 mo, two articles proposed mathematical models to explain cell migration. In these models, plasma membrane area and plasma membrane tension emerge as two critical parameters to support their conclusions (Ji *et al*., 2008; Keren *et al*., 2008). We think that our results provide the direct observation and proof of

what really appends in the cells and how those two parameters are modulated in vivo. This is an important step forward in the field showing that more than any change in protein or lipid composition, a simple change in the total plasma membrane area could lead to modifications in cell behavior. We also think that our study clarifies why dozens of molecules described to regulate membrane trafficking have been at one point described to modulate cell migration. In conclusion, we propose that the plasma membrane area is a critical biophysical parameter during cell shape changes.

ACKNOWLEDGMENTS

We thank all the members of the Sheetz laboratory for support and help. N.C.G. designed experiments, performed experiments, and wrote the article. O.M.R. designed experiments and performed experiments. A. M. and J.C.H. helped for the microcontact printing, and M.P.S. supervised the work. This work was supported by National Institutes of Health grant GM-064561 (to M.P.S.).

REFERENCES

Andrews, N. W., and Chakrabarti, S. (2005). There's more to life than neurotransmission: the regulation of exocytosis by synaptotagmin VII. Trends Cell Biol. *15*, 626–631.

Balasubramanian, N., Scott, D. W., Castle, J. D., Casanova, J. E., and Schwartz, M. A. (2007). Arf6 and microtubules in adhesion-dependent trafficking of lipid rafts. Nat. Cell Biol. *9*, 1381–1391.

Benmerah, A., and Lamaze, C. (2007). Clathrin-coated pits: vive la difference? Traffic *8*, 970–982.

Bergmann, J. E., Kupfer, A., and Singer, S. J. (1983). Membrane insertion at the leading edge of motile fibroblasts. Proc. Natl. Acad. Sci. USA *80*, 1367–1371.

Boucrot, E., and Kirchhausen, T. (2007). Endosomal recycling controls plasma membrane area during mitosis. Proc. Natl. Acad. Sci. USA *104*, 7939–7944.

Bretscher, M. S., and Aguado-Velasco, C. (1998). Membrane traffic during cell locomotion. Curr. Opin. Cell Biol. *10*, 537–541.

Brumback, A. C., Lieber, J. L., Angleson, J. K., and Betz, W. J. (2004). Using FM1-43 to study neuropeptide granule dynamics and exocytosis. Methods *33*, 287–294.

Cai, Y., *et al*. (2006). Nonmuscle myosin IIA-dependent force inhibits cell spreading and drives F-actin flow. Biophys. J. *91*, 3907–3920.

Champion, J. A., and Mitragotri, S. (2006). Role of target geometry in phagocytosis. Proc. Natl. Acad. Sci. USA *103*, 4930–4934.

Chen, C. S., Mrksich, M., Huang, S., Whitesides, G. M., and Ingber, D. E. (1997). Geometric control of cell life and death. Science *276*, 1425–1428.

Coupin, G. T., Muller, C. D., Remy-Kristensen, A., and Kuhry, J. G. (1999). Cell surface membrane homeostasis and intracellular membrane traffic balance in mouse L929 cells. J. Cell Sci. *112*, 2431–2440.

Dai, J., and Sheetz, M. P. (1995). Axon membrane flows from the growth cone to the cell body. Cell *83*, 693–701.

Dai, J., and Sheetz, M. P. (1998). Cell membrane mechanics. Methods Cell Biol. *55*, 157–171.

del Pozo, M. A., Alderson, N. B., Kiosses, W. B., Chiang, H. H., Anderson, R. G., and Schwartz, M. A. (2004). Integrins regulate Rac targeting by internalization of membrane domains. Science *303*, 839–842.

Dubin-Thaler, B. J., Giannone, G., Dobereiner, H. G., and Sheetz, M. P. (2004). Nanometer analysis of cell spreading on matrix-coated surfaces reveals two distinct cell states and STEPs. Biophys. J. *86*, 1794–1806.

Dyer, N., Rebollo, E., Dominguez, P., Elkhatib, N., Chavrier, P., Daviet, L., Gonzalez, C., and Gonzalez-Gaitan, M. (2007). Spermatocyte cytokinesis requires rapid membrane addition mediated by ARF6 on central spindle recycling endosomes. Development *134*, 4437–4447.

Gagnon, E., Duclos, S., Rondeau, C., Chevet, E., Cameron, P. H., Steele-Mortimer, O., Paiement, J., Bergeron, J. J., and Desjardins, M. (2002). Endoplasmic reticulum-mediated phagocytosis is a mechanism of entry into macrophages. Cell *110*, 119–131.

Gauthier, N. C., Monzo, P., Kaddai, V., Doye, A., Ricci, V., and Boquet, P. (2005). *Helicobacter pylori* VacA cytotoxin: a probe for a clathrin-independent and Cdc42-dependent pinocytic pathway routed to late endosomes. Mol. Biol. Cell *16*, 4852–4866.

Giannone, G., Dubin-Thaler, B. J., Dobereiner, H. G., Kieffer, N., Bresnick, A. R., and Sheetz, M. P. (2004). Periodic lamellipodial contractions correlate with rearward actin waves. Cell *116*, 431–443.

Giannone, G., *et al*. (2007). Lamellipodial actin mechanically links myosin activity with adhesion-site formation. Cell *128*, 561–575.

Herring, T. L., Slotin, I. M., Baltz, J. M., and Morris, C. E. (1998). Neuronal swelling and surface area regulation: elevated intracellular calcium is not a requirement. Am. J. Physiol. *274*, C272–C281.

Hochmuth, F. M., Shao, J. Y., Dai, J., and Sheetz, M. P. (1996). Deformation and flow of membrane into tethers extracted from neuronal growth cones. Biophys. J. *70*, 358–369.

Honig, M. G., and Hume, R. I. (1989). Carbocyanine dyes. Novel markers for labelling neurons. Trends Neurosci. *12*, 336–338.

Itano, N., Okamoto, S., Zhang, D., Lipton, S. A., and Ruoslahti, E. (2003). Cell spreading controls endoplasmic and nuclear calcium: a physical gene regulation pathway from the cell surface to the nucleus. Proc. Natl. Acad. Sci. USA *100*, 5181–5186.

Jaiswal, J. K., Andrews, N. W., and Simon, S. M. (2002). Membrane proximal lysosomes are the major vesicles responsible for calcium-dependent exocytosis in nonsecretory cells. J. Cell Biol. *159*, 625–635.

Ji, L., Lim, J., and Danuser, G. (2008). Fluctuations of intracellular forces during cell protrusion. Nat. Cell Biol. *10*, 1393–1400.

Jones, M. C., Caswell, P. T., and Norman, J. C. (2006). Endocytic recycling pathways: emerging regulators of cell migration. Curr. Opin. Cell Biol. *18*, 549–557.

Kehle, T., and Herzog, V. (1989). A colloidal gold labeling technique for the direct determination of the surface area of eukaryotic cells. Eur. J. Cell Biol. *48*, 19–26.

Keren, K., Pincus, Z., Allen, G. M., Barnhart, E. L., Marriott, G., Mogilner, A., and Theriot, J. A. (2008). Mechanism of shape determination in motile cells. Nature *453*, 475–480.

Kneen, M., Farinas, J., Li, Y., and Verkman, A. S. (1998). Green fluorescent protein as a noninvasive intracellular pH indicator. Biophys. J. *74*, 1591–1599.

Kuo, S. C., and Sheetz, M. P. (1992). Optical tweezers in cell biology. Trends Cell Biol. *2*, 116–118.

Kuo, S. C., and Sheetz, M. P. (1993). Force of single kinesin molecules measured with optical tweezers. Science *260*, 232–234.

Li, R., *et al*. (2003). On the same cell type GPI-anchored normal cellular prion and DAF protein exhibit different biological properties. Biochem. Biophys. Res. Commun. *303*, 446–451.

Lippincott-Schwartz, J., Yuan, L. C., Bonifacino, J. S., and Klausner, R. D. (1989). Rapid redistribution of Golgi proteins into the ER in cells treated with brefeldin A: evidence for membrane cycling from Golgi to ER. Cell *56*, 801–813.

Lippincott-Schwartz, J., and Zaal, K. J. (2000). Cell cycle maintenance and biogenesis of the Golgi complex. Histochem. Cell Biol. *114*, 93–103.

Matteoni, R., and Kreis, T. E. (1987). Translocation and clustering of endosomes and lysosomes depends on microtubules. J. Cell Biol. *105*, 1253–1265.

Mayor, S., and Pagano, R. E. (2007). Pathways of clathrin-independent endocytosis. Nat. Rev. Mol. Cell Biol. *8*, 603–612.

Morris, C. E., and Homann, U. (2001). Cell surface area regulation and membrane tension. J. Membr. Biol. *179*, 79–102.

Naslavsky, N., Weigert, R., and Donaldson, J. G. (2004). Characterization of a nonclathrin endocytic pathway: membrane cargo and lipid requirements. Mol. Biol. Cell *15*, 3542–3552.

Neves, S. R., *et al*. (2008). Cell shape and negative links in regulatory motifs together control spatial information flow in signaling networks. Cell *133*, 666–680.

Peterson, J. R., and Mitchison, T. J. (2002). Small molecules, big impact: a history of chemical inhibitors and the cytoskeleton. Chem. Biol. *9*, 1275–1285.

Proux-Gillardeaux, V., Gavard, J., Irinopoulou, T., Mege, R. M., and Galli, T. (2005). Tetanus neurotoxin-mediated cleavage of cellubrevin impairs epithelial cell migration and integrin-dependent cell adhesion. Proc. Natl. Acad. Sci. USA *102*, 6362–6367.

Rappoport, J. Z., and Simon, S. M. (2003). Real-time analysis of clathrin-mediated endocytosis during cell migration. J. Cell Sci. *116*, 847–855.

Raucher, D., and Sheetz, M. P. (2000). Cell spreading and lamellipodial extension rate is regulated by membrane tension. J. Cell Biol. *148*, 127–136.

Reddy, A., Caler, E. V., and Andrews, N. W. (2001). Plasma membrane repair is mediated by Ca(2+)-regulated exocytosis of lysosomes. Cell *106*, 157–169.

Rodriguez, A., Webster, P., Ortego, J., and Andrews, N. W. (1997). Lysosomes behave as Ca2+-regulated exocytic vesicles in fibroblasts and epithelial cells. J. Cell Biol. *137*, 93–104.

Schmoranzer, J., Goulian, M., Axelrod, D., and Simon, S. M. (2000). Imaging constitutive exocytosis with total internal reflection fluorescence microscopy. J. Cell Biol. *149*, 23–32.

Schmoranzer, J., Kreitzer, G., and Simon, S. M. (2003). Migrating fibroblasts perform polarized, microtubule-dependent exocytosis towards the leading edge. J. Cell Sci. *116*, 4513–4519.

Schmoranzer, J., and Simon, S. M. (2003). Role of microtubules in fusion of post-Golgi vesicles to the plasma membrane. Mol. Biol. Cell *14*, 1558–1569.

Sheetz, M. P., Sable, J. E., and Dobereiner, H. G. (2006). Continuous membrane-cytoskeleton adhesion requires continuous accommodation to lipid and cytoskeleton dynamics. Annu. Rev. Biophys. Biomol. Struct. *35*, 417–434.

Small, J. V., Geiger, B., Kaverina, I., and Bershadsky, A. (2002). How do microtubules guide migrating cells? Nat. Rev. Mol. Cell Biol. *3*, 957–964.

Smith, C. B., and Betz, W. J. (1996). Simultaneous independent measurement of endocytosis and exocytosis. Nature *380*, 531–534.

Strickland, L. I., and Burgess, D. R. (2004). Pathways for membrane trafficking during cytokinesis. Trends Cell Biol. *14*, 115–118.

Touret, N., *et al*. (2005). Quantitative and dynamic assessment of the contribution of the ER to phagosome formation. Cell *123*, 157–170.

Traynor, D., and Kay, R. R. (2007). Possible roles of the endocytic cycle in cell motility. J. Cell Sci. *120*, 2318–2327.